CHAPTER THREE

Methylene blue-eluting nanofibers as a potential biomaterial for antimicrobial photodynamic therapy (APDT)

1. Introduction

Antimicrobial nanofibers are rapidly evolving as a biomaterial for the control of microbial growth in diverse biomedical applications involving cell regeneration. They have been widely investigated in recent years as wound dressings materials [6, 106, 342], medical and protective personal hygienic textiles with barrier properties to microorganisms and viruses [343], sutures [344], membranes to prevent tissue adhesion post abdominal surgery [132], facial masks for antimicrobial protection [345] and personal care [346], and coating materials for medical devices [347]. The antimicrobial effect of nanofibers can be achieved by loading the fibers matrix with low molecular weight antimicrobial agents such as antibiotics [46, 105, 348, 349], antibacterial agents [259, 350] or biocides [351] for temporally controlled relatively short term drug delivery or by using antimicrobial polymers with non-leachable functional moieties for permanent antimicrobial applications [352, 353].

The functionality of antimicrobial NFs can be further enhanced by integrating advances in materials science and antimicrobial techniques. For instance, the use of responsive polymers for the fabrication of stimuli-responsive NFs allows triggered release of encapsulated drugs in response to external stimuli such as pH, temperature, magnetic field, ultrasound energy and UV radiation [354]. Further, merging the structural and functional potentials of antimicrobial NFs as a biomaterial with the effectiveness of an antimicrobial technique such as photodynamic activation may provide a novel combined platform for more effective antimicrobial photodynamic therapy (APDT) applications.

The activity of APDT is based on the photodynamic process induced by the irradiation of a photosensitizer (PS) with light at specific wavelengths, producing a series of reactive species, the actual effectors of this antimicrobial therapeutic modality [2, 3]. During photoactivation, the PS molecule reaches a higher energy level, known as the first excited singlet state. Return of this singlet state to its ground state is associated with emission of fluorescence or, by intersystem crossing, it can be converted to a long-lived triplet state, which enables the triplet-PS to chemically interact with molecules in the surroundings [4]. To return to its ground state, the triplet PS can transfer energy directly to biomolecules present in the environment (type I reaction) or, alternatively, it transfers energy to triplet oxygen, producing mainly singlet oxygen, a reactive oxygen species (ROS) about 1000-fold more oxidant than triplet oxygen (Type II reaction). The main PDT effect is attributed to a type II reaction. Each photosensitizer molecule can typically produce 10^3–10^5 molecules of $^1O_2$ [13]. Highly reactive oxygen is extremely electrophilic and initiates further oxidative damage to biomolecules in the proximate environment, such as the bacterial cell wall, lipid membranes, enzymes, or nucleic acids [145]. The degradation of microbial biomolecules eventually leads to microbial cell death. The ROS produced during PDT react non-specifically with several biomolecules such as lipids, nucleic acids and proteins only near the site of photo-activation. Thus, as the ROS attack may occur at several different sites within a molecule, the biomolecules are non-specifically damaged, a feature precluding the generation of mutant PDT-resistant microbial strains [162]. In fact, as a result of their high reactivity, ROS generated during PDT have a very short half-life, in the microseconds range and can then diffuse only through very short distances [6, 7].

APDT is generally safe with few side effects because of its double specificity achieved by both of the light-mediated targeting of therapy to the irradiated infected area and the microbial cell-affinity targeting of the PS as a result of its higher affinity for prokaryotic microbial cells compared to human eukaryotic cells [24-27]. While antibiotics take several days to act, microbial inactivation by APDT is instantaneous. The therapeutic window of APDT is broader than other antimicrobial therapies, even against pathogenic biofilms [177]. Besides, It can be used to treat damaged or dead tissue, e.g. burns [178, 179]. APDT has been used in dental applications such as periodontitis [355], root canal disinfection [356], gingivitis [357] and oral candidiasis [358] due to easy access of the light source to the mouth. Other medical applications of APDT include acne and infections resulting from burns [178, 179], surgical wounds [197] or soft-tissue infections [198]. Clinical findings revealed that APDT is a promising treatment against a variety of infectious microbes *in vivo.*

It has been reported that encapsulation of PS in a polymeric matrix enhances photodynamic activity by preventing the PS molecular association to form dimers, trimers and higher aggregates which reduce photodynamic activity [28, 29]. In addition, encapsulation enhances the solubility of hydrophobic PS [209]. Different PSs delivery systems were used to enhance APDT for diverse applications. For instance, liposomes have been used to target the PS to the prokaryotic rather than eukaryotic cells [210], to reduce the ability of the target cell to pump out the PS, hence reducing the possibility of multidrug resistance [211] and to treat acne [213]. Solid lipid nanoparticles [359] and polymer nanoparticles [219] were used to treat dental plaque. PSs-loaded membranes have been applied for disinfection of implanted catheters [201-203]. In this context, the use of electrospun matrices as a delivery system for photosensitizers for photodynamic applications has not been explored yet. The mechanism of photoactivation of PS-eluting NFs would depend on the delivery of water soluble PS into the infected site and PS binding to target bacterial cells prior to irradiation. Accordingly, apart from parameters inherent to photodynamic activation, synchronization of light irradiation with PS release is a main determinant of antimicrobial photodynamic activity. This release-dependent photodynamic activity approach is different from a previously reported approach based on immobilization of hydrophobic PS in a polymer NFs matrix [48]. Inactivation of bacteria by these photoactive NFs depends on the transport of the light-generated singlet oxygen within the fibers matrix to bacteria adhering to the NF surface. To date, a few studies have been reported on photoactive light transparent NFs focusing on surface photoactivation of NFs doped with tetraphenylporphyrin and/or zinc phthalocyanine as PSs. *In vitro* antimicrobial assessment indicated that the type of polymer, light transmission through the fiber matrix and NFs diameter are the main factors affecting antimicrobial photoactivity. The non-shed PS on the large surface area of nanofibrous matrices showed the ability to kill bacteria on NFs surfaces when exposed to visible light [48, 225, 226]. A single study reported the exploration of such photoactive textiles in the setting of chronic wound healing [227].

In chapter one of the thesis, we developed MB-loaded PHB/PEG NFs as an antimicrobial biomaterial for biomedical applications. The NFs showed a biphasic release profile of MB and antimicrobial activity against two test organisms commonly found in infected wounds which suggest their suitability for short term antimicrobial applications, particularly wound healing. Photoactivation of these NFs would enhance their antimicrobial effect and wound healing properties. The antimicrobial effect exerted by MB in the dark can be augmented, at oxygenated environment, by the incidence of light with a wavelength corresponding to its electronic

absorption band, 660 nm [45, 46]. Irradiation of MB in dilute aqueous solutions where no dimers are present, results in the generation of triplets with high quantum yield (ϕ_T = 0.52), and high singlet oxygen quantum yield $\phi_\Delta \sim$ 0.5 [44, 47]. These photophysical properties in the therapeutic window, coupled with MB solubility, cationic nature, low toxicity, low reduction potential and intense light absorption makes MB an effective antimicrobial photosensitizer for APDT [10, 13, 43, 44, 47].

The objective of this chapter of the thesis was to evaluate MB-eluting NFs as a multifunctional carrier system for the controlled delivery of PS antimicrobial/photosensitizer for APDT using LED at 650 nm. The non-coherent Light-emitting diode (LED) array has been selected as the light source because of the safety of LEDs, their high selectivity, low cost, easy configuration on small chips and reported similarity of their effects on wound healing to that of coherent laser [170, 173, 360, 361]. To get insight into the photoactivation process, the effect of the photophysical properties of the PHB/PEG nanofibrous matrix, the light dose and MB concentration on the process were assessed to determine the optimum conditions for effective antimicrobial photodynamic activation of MB-eluting NFs against two test microorganisms, *S. aureus* and MRSA.

2. Materials and Methods

2.1. Materials

Chemicals

- Methylene blue (MB) (Aldrich chemical co. Ltd., England)
- Polyhydroxybutyrate (PHB, 250 kDa, Nantian Co. Ltd., Jiangsu, China)
- Polyethylene glycol 4000 (PEG 4000) (Fluka AG, Buchs SG, Switzerland)
- Span 80 (Guang dong Guanghua chemical factory Co. Ltd., China)
- Uric acid (Oxford Laboratory, Maharashtra, India)
- Chloroform (Sigma-Aldrich, UK)
- Ethanol Absolute (Sigma-Aldrich, Munich, Germany)
- Sodium chloride (Adwic, El-Nasr Pharmaceutical Co., Abuzaabal, Egypt)
- Potassium dihydrogen orthophosphate and sodium hydrogen phosphate dibasic (WINLAB, Leicestershire, UK)

Culture Media

Nutrient agar and nutrient broth (Oxoid Ltd; Basingostok; Hampshire, England).

Microorganisms:

Methicillin resistant *Staphylococcus aureus* (MRSA) clinical isolate and a standard strain of *Staphylococcus aureus* ATCC 6538P (Sa_{st}) were obtained from the Department of Pharmaceutical Microbiology, Faculty of Pharmacy, University of Alexandria.

2.2. Equipment

- Electrospinning apparatus equipped with High Voltage DC Power Supply(P3508, Raymax, Canada) and a syringe pump (101, KD scientific, USA)
- Vortex mixer (VM-300, KK, USA)
- Digital heated sonicator (UD100SH-3L, Eumax, Hong Kong)
- High speed cooling centrifuge (3-30k, Sigma Laborzentrifugen, Germany)
- Adventurer sensitive electrical digital balance (Ohause Corp. Pine Brook, NJ, USA).
- Hot plate magnetic stirrer (IP 21, IKA, Staufen, Germany)
- UV-Visible Spectrophotometer (T80 UV/ Vis PG Instruments Spectrophotometer. ltd, England).
- pH-meter (pH 211, Hanna Instruments, Rhode Island, USA).
- Micrometer (IP 65, Mitutoyo Manufacturing, Tokyo, Japan)
- Digital camera, 12 mega pixels, 5X optical zoom (ES70, Samsung Co, South Korea).
- Programmable LED power supply with 24 lamp (assembled in-house)
- Scanning electron microscope (JSM-5300, JEOL, Japan).
- Ion sputtering coater (JFC-1100E, JEOL, Japan).
- Incubator (BST 5020, MLW, Germany)

- Portable autoclaves (A. Gallenkamp & Co. Ltd, UK).
- Micropipettes (Comecta, Spain).

2.3. Methods

2.3.1. The light source

The light source used in the study was a 24 lamp-light emitting diode (LED) array (4 x 6 non-coherent lamps), generating a light beam with 650 nm peak wavelength overlapping the absorbance maximum of methylene blue in aqueous solution (660 nm). The emitted beam has an intensity of 150 mW and covers an area of 1.7 cm diameter. The array is shown in Figure 44.

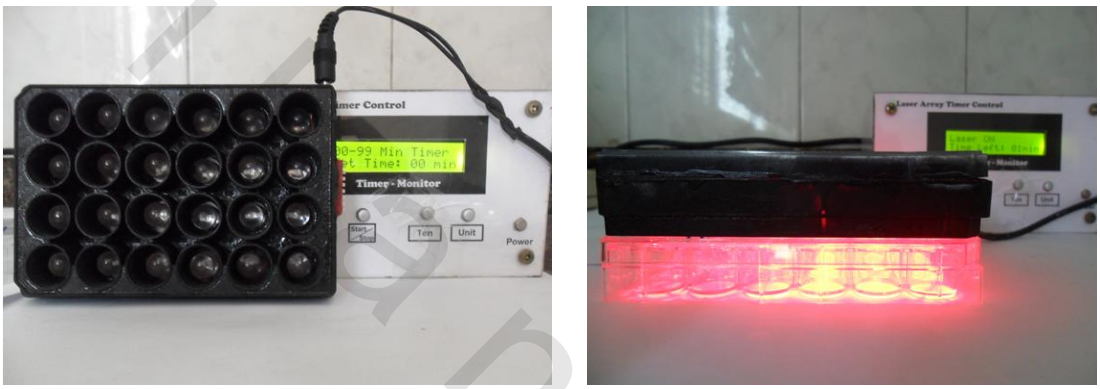

Figure 44: The 24 lamp-Light Emitting Diode (LED) array

The required light dose or fluence can be calculated using the following equation:

$$\text{Fluence (J/cm}^2\text{)} = \text{light irradiance (W/cm}^2\text{)} \times \text{time (sec)} \quad [362]$$

2.3.2. Investigation of the photodynamic activation of MB-PHB/PEG nanofibers

2.3.2.1.Light absorption and transmittance by MB-PHB/PEG nanofibers

In a preliminary investigation, the effect of PHB/PEG polymer matrix on the spectral characteristics of MB was assessed by recording the visible absorption spectra of MB in aqueous solutions of different concentrations and the spectra of MB-PHB/PEG nanofibers mesh and a MB-loaded PHB/PEG non-porous cast film with the same polymer composition as reported previously for polyurethane and silicone samples [203]. The NFs mesh (0.9 x 3 cm, 350 µm thick) or the film (0.9 x 3 cm, 350 µm thick) was fitted longitudinally to the cuvette of the spectrophotometer. The visible absorption spectra of plain PHB/PEG nanofibers and a plain cast film were also recorded for comparison.

Further, the transmittance of emitted light at 650 nm across the MB-loaded PHB/PEG NFs samples was assessed as a function of sample thickness (150 to 500 µm, as measured with a micrometer) and sample wetting with PBS (treatment time ranging from 0.5 to 90 min).

2.3.2.2. Photodynamic activation of MB released from PHB/PEG nanofibers

The photodynamic activity of MB released from PHB/PEG NFs, expressed as singlet oxygen, was assessed using the uric acid (UA) method [363-365]. The method is based on measuring the decrease in UA absorbance at λmax 293 nm (UA-A_{293}) as a result of UA quenching of singlet oxygen generated by irradiation of MB in a solution containing UA.

A fresh stock solution of uric acid was made up in PBS at a concentration of 120 µg/ml by dissolving UA by repeated vortexing one hour prior to the assay. A working stock UA solution 60 µg/ml in PBS was prepared immediately. Air was pumped into the solution for 5 min to ensure air-saturation and availability of sufficient oxygen.

As MB absorbance at 293 nm (MB second peak at 292 nm) can interfere with UA absorbance, the MB concentration range within which MB interference was minimal was determined. A series of standard MB solutions in PBS (2 - 12 µg/ml) were irradiated for different durations, 12.5, 25, 50, 75 and 100 min corresponding to a fluence of 50, 100, 200, 300 and 400 J/cm^2 respectively. The MB concentration range determined was considered in the assessment of singlet oxygen generation in subsequent experiments.

For the assessment of photodynamic activity of MB released from PHB/PEG nanofibers, a release experiment was conducted by placing a sample of MB-loaded NFs weighing 24 mg and containing ≈ 120 µg MB (calculated based on sample weight and E.E. %) in 50 ml stoppered conical flasks containing 12 ml PBS pH 7.4 as release medium. Flasks were shaken in a thermostatically controlled water bath adjusted to 37°C at 30 strokes /minute. The release experiment was terminated at different time intervals (0.25, 0.5, 1, 2, 4 and 6 h). Samples of release media of terminated experiments, 1.5 ml each, were transferred to individual wells of a 24 well tissue culture plate and 1.5 ml of the UA solution 60 µg/ml was added. A set of three samples obtained at each time interval were irradiated using the LED array for 25 and 50 minute corresponding to 100 and 200 J/cm^2. A control set of samples was kept in the dark after addition of UA. Absorbance of UA in all cases was measured at 293 nm. The difference between absorbance of control and irradiated samples was calculated. Data were expressed as the average change in UA-A_{293}.

2.3.3. Photodynamic antimicrobial activity of MB-eluting nanofibers

The antibacterial photodynamic activity (APDA) of MB-eluting PHB/PEG NFs was assessed using two bacterial strains, *Staphylococcus aureus* standard strain (Sa_{st}) and MRSA. Assessment was based on irradiation of MB released from NFs.

2.3.3.1. Effect of experimental variables on the APDA of MB solution

In a screening study, experimental variables, namely MB concentration, light fluence and pre-irradiation incubation time were modulated in order to maximize the APDA of MB solution. For the effect of MB solution concentration, a 200 µl aliquot of a diluted overnight culture (~10^6 CFU/ml) of the test organism was added to 200 µl of MB solution of different concentrations in sterile saline in a 24-well sterile plate with a lid, giving final MB concentrations ranging from 6.25 to 100 µg/ml for MRSA and from 25 to 200 µg/ml for Sa_{st}. The plate was incubated at 37° C with shaking at 75 stroke/min for 30 min. Test wells were irradiated with the LED array positioned vertically above the wells so that each well was irradiated with one LED lamp. Control samples were protected from light in another plate. The light fluence ranged from 30 to 200 J/cm^2 for MRSA and from 100 to 200 J/cm^2 for Sa_{st}. After irradiation of test wells, 100 µl-samples of the mixture were removed and serially diluted tenfold in sterile saline. Aliquots, 20 µl each, of the undiluted and diluted samples were plated out on nutrient agar and the total viable count determined after overnight incubation at 37 °C. A positive control group was prepared by adding 200 µl of bacterial culture to 200 µl of sterile saline.

The effect of incubation time on the APDA of MB was tested using MRSA and MB at two concentrations, 25 and 50 µg/ml. Aliquots, 200 µl each, of a diluted overnight MRSA culture (~10^6 CFU/ml) were added to the wells of a 24-well plate and 200 µl of either sterile saline (control) or sterile saline containing MB of known concentration were added to give final MB concentrations of 25 and 50 µg/ml. Mixtures were incubated for zero, 5, 15 and 30 min at 37°C with shaking at 75 strokes/min and then either subjected to irradiation with LED at 650 nm (fluence 100 J/cm^2) or kept in the dark (control) for the same duration. Zero incubation time samples were irradiated immediately after addition of MB solution to the bacterial suspension. Total viable count was performed as described previously. All experiments were carried out in duplicate and the results were expressed as mean survival bacterial count (CFU/ml).

2.3.3.2. Antibacterial photodynamic activity (APDA) of MB released from PHB/PEG nanofibers

Based on data obtained above for modulation of experimental variables, the APDA of MB released from PHB/PEG NFs at 15 min was assessed against *Sa_{st}* and MRSA. Circular NFs meshes (≈ 12 mg and 1 cm diameter) with known MB content were placed inside the individual wells of a 24-well plate. Aliquots (200 µl) of bacterial cultures (~10^6 CFU/ml) of the test organisms were added to each well followed by 200 µl of sterile saline. Wells were irradiated with LED 650 nm at a fluence of 100 J/cm^2. A similar set (control) was prepared in another 24-well plate kept in the dark. The APDA of MB released from NFs at 15 min was compared with that of a MB solution of equal concentration. Bacterial count was performed immediately as described previously. All experiments were carried out in triplicate and the results were expressed as mean survival bacterial count (CFU/ml).

2.3.3.3.Antibacterial profile of light activated MB-eluting nanofibers

The same procedure was used to test for possible bacterial recovery following treatment of bacteria with MB-eluting NFs and light for 24 h. Nutrient broth rather than saline was used to dilute the bacterial cultures in NFs-containing wells to support bacterial growth. Wells were irradiated as described above. Aliquots were aspirated from a set of wells immediately after irradiation for bacterial counting while another set was kept in the dark for 24 h following irradiation before bacterial counting. Positive control systems were prepared by mixing 200 µl of bacterial culture (~10^6 CFU/ml) with 200 µl of nutrient broth. All experiments were carried out in triplicate and the results were expressed as mean survival bacterial count (CFU/ml).

3. Results and Discussion

In chapter one of the thesis, electrospun MB-loaded PHB/PEG NFs made of a PHB/PEG polymer blend (3: 2) and fabricated by emulsion electrospinning were developed for biomedical applications. The NFs were characterized by a smooth surface, a mean diameter of 411 nm and a loading efficiency of 5 mg/g of polymer. The MB release profile was biphasic, allowing fast initial MB release (33% approximately in the first hour) associated with slower diffusion-controlled release reaching 90% in 7 days. Based on these data, MB-loaded PHB/PEG NFs offer great potentials as a biomaterial for relatively short duration antimicrobial biomedical applications, particularly wound healing. These NFs combines the well-established wound healing accelerating effects of NFs and the dual antimicrobial activity of MB as antimicrobial agent and photosensitizer susceptible to light activation and hence to enhancement of the MB-NFs efficiency. In this chapter, the effect of light emitted at 650 nm by a Light Emitting Diode (LED) at 650 nm on the spectral characteristics, photoactivity and photodynamic antimicrobial activity of MB-eluting NFs was investigated.

Figure 45 shows a digital photograph and a SE micrograph of the MB-loaded NFs mat under study. The mat appears lightly blue-colored and opaque indicating encapsulation of MB inside the NFs matrix.

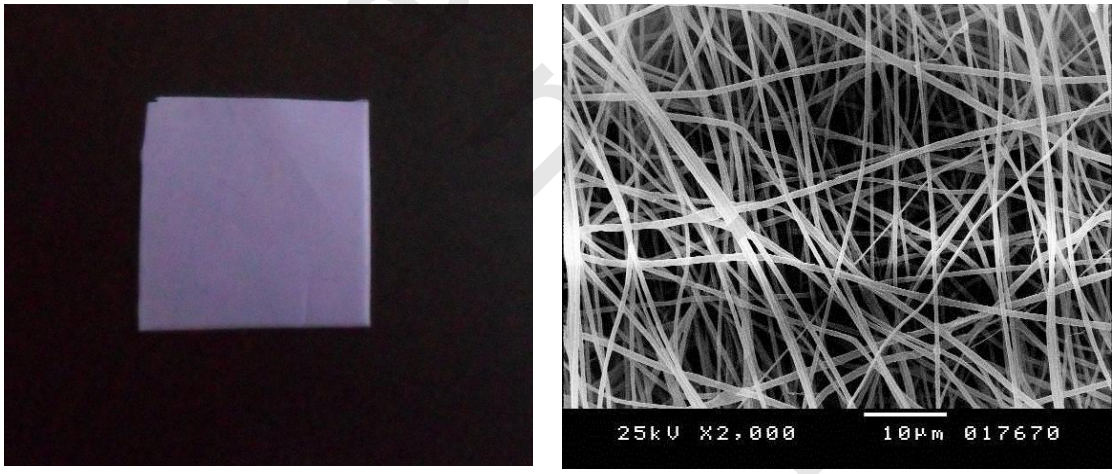

Figure 45: Digital photograph and scanning electron micrograph of MB-eluting PHB/PEG NFs

3.1. Light absorption and transmittance by MB-PHB/PEG nanofibers

The effect of the PHB/PEG polymer nanofibrous structure on the spectral characteristics of MB was investigated by comparing qualitatively the visible absorption spectra of MB-PHB/PEG nanofibers mesh and a MB-loaded PHB/PEG unstructured cast film having the same polymer composition and MB loading with the spectrum of MB in aqueous solution. NFs and film samples were fitted longitudinally to the spectrophotometer cuvette. Spectra for plain PHB/PEGNFs and a MB-loaded non-porous cast film with a similar polymer composition were recorded for comparison. The visible spectra of MB solutions (Figure 46a) show a prominent

absorption peak at ≈ 660 nm, a hump at ≈ 614 nm and a second peak at 292 nm. Incorporation of MB in PHB/PEG polymer blend NFs resulted in a change in absorption characteristics, including mainly a change in the shape of the main absorption band at 660 nm and increased absorption intensity throughout the spectrum (Figure 46b). No additional peaks appeared indicating absence of MB aggregates in the polymer matrix, an important observation in view of the poor ability of dimers or higher aggregates of photosensitizers to produce singlet oxygen, $^1O_2$ [366]. Interaction of MB with PHB through hydrogen bonding and electrostatic interaction as verified by FT-IR in Chapter one of the thesis and shielding of MB by the non-transparent NFs polymer matrix accounted at least in part for the change in MB peak characteristics. The spectral characteristics of MB and other dyes embedded in a polymer matrix were shown to change depending on the polymer type and swelling properties [202, 203]

Interestingly, absorption intensity of NFs samples was much greater than that of the corresponding unstructured films with the same polymer composition. This can be attributed to the structural features of the NFs mesh. As pointed out by Chang group [367], the nanofibrous structure enhances light scattering and propagation with prolongation of the light path lengths in the matrix. This was accounted for by the curved and randomly-oriented features of single NFs in a non-oriented mesh which can only support momentary light confinement, inducing multiple light scattering events. Light scattering in NFs, responsible for their white color in most instances, was shown to depend on the NF diameter and mesh thickness. The enhanced light scattering phenomenon observed in NFs rendered them potential light trapping and propagation matrices as optical filters [368].

Light absorption properties of NFs were verified by light transmittance (T) data obtained for the MB-PHB/PEG NFs under study. Table 13 shows that T by the 500 µm-thick NFs mat in the dry state was low (0.1 %), supporting the enhanced light scattering ability of NFs. Reducing the mat thickness resulted in a slight increase in % T. For example, the increase in % T corresponding to the decrease in the mat thickness from 500 to 150 was 0.3%. However, wetting NFs samples by treating the mats with PBS pH 7.4 at 37^{o}C resulted in a larger, though limited, increase in %T, effect being generally dependent on the treatment time. For instance, brief immersion of the thinnest NFs sample (150 µm) in PBS resulted in 4.4-fold increase in % T (1.33 %) while increasing PBS treatment time to 90 min resulted in a 7.7-fold increase (2.3 %). Wetting rendered the polymer matrix more light-transparent. Results indicated that light scattering by the NFs structure hinders light transmission. Results were consistent with those reported for carbon nanofibers in implying that the NFs network changes the pathway of the transmitted light causing large fraction of light to be lost through diffraction and scattering [369]. Combined light absorption and transmission data suggested poor transparency of PHB/PEG NFs to incident light which might have important implications in different biomedical and other applications. As far as applications based on light-activated antimicrobial activity are concerned, data obtained implied protection of MB encapsulated in PHB/PEG NFs against photosensitization and dependence of light activated antimicrobial activity mainly on released rather entrapped MB. Corroborating data have been obtained by McCarthy *et al* [370] who reported quenching of the excited state and phototoxicity of MB encapsulated within PLGA nanoparticles with regain of MB activity upon release from nanoparticles incubated with cells.

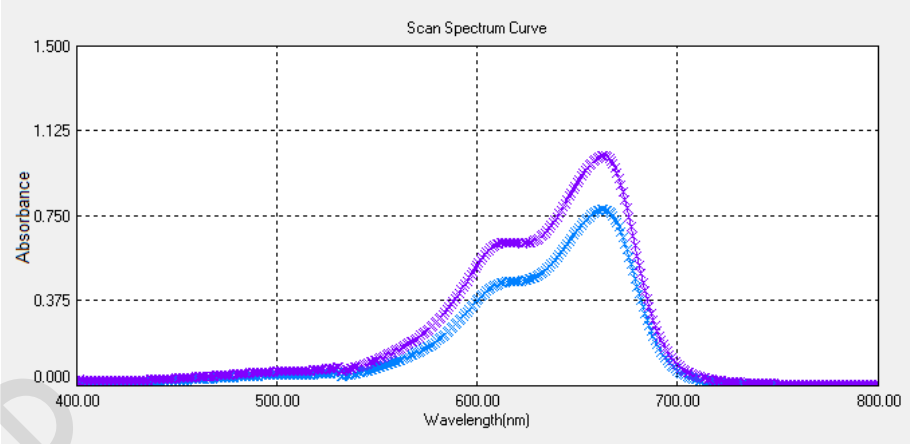

Figure 46a: Visible Spectra of MB aqueous solutions (5 and 7 µg/ml).

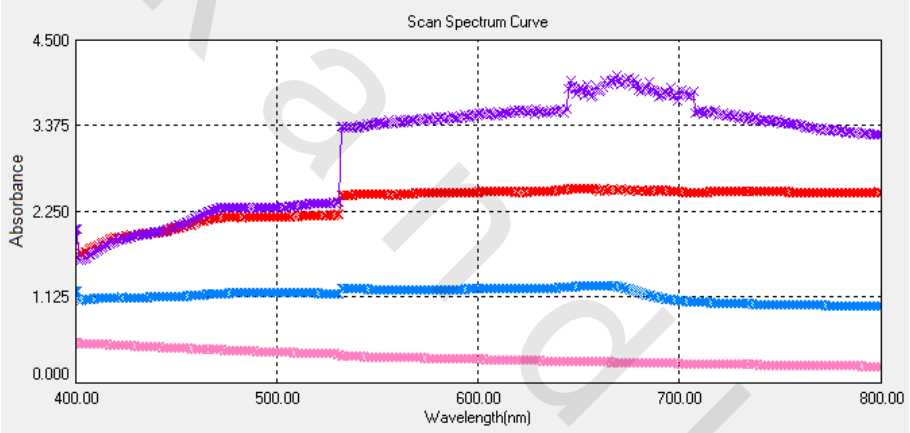

Figure 46b: Visible Spectra of MB-loaded and plain NFs vs. films; MB-loaded NFs (violet), plain NFs (red), MB-loaded film (blue) and plain film (pink) as reported [203].

Table 13: Effect mat thickness and treatment with PBS on the light transmittance (T %) at 650 nm of MB-loaded PHB/PEG nanofibers (n = 3)

NF mesh thickness (µm)	Transmission % of NFs mesh after treatment with PBS pH 7.4 at 37 °C			
	PBS treatment time			
	Zero	0.5 min	30 min	90 min
500	0.1± 0.0	0.6±0.26	0.8±0.10	0.8±0.10
350	0.1± 0.0	0.6±0.10	0.8±0.26	0.7±0.17
220	0.2±0.1	0.7±0.10	0.8±0.20	1.3 ±0.15
150	0.3±0.1	1.3±0.15	1.2±0.26	2.3±0.36

3.2. Photodynamic activation of MB released from PHB-PEG nanofibers

(Uric acid method for determination of singlet oxygen ($^1O_2$) generated by photoactivation of MB with LED 650 nm)

As the photodynamic activity of MB-PHB/PEG NFs depends on photosensitization of released MB, experimental variables affecting photodynamic activity of MB solution such as MB concentration and light fluence were investigated. Singlet oxygen assay based on the uric acid (UA) method [364, 365] that was firstly developed by Fischer *et al* [363] and was used for the assay of MB photoactivity by Perni *et al* [202]. The assay depends on estimation of singlet oxygen species, $^1O_2$, generated upon irradiation of a photosensitizer. In the present study, MB was irradiated with a light emitting diode (LED) emitting red light at 650 nm, a wavelength overlapping with MB wavelength of maximum absorption. The test depends on oxidation of UA by $^1O_2$ generated by photosensitizer irradiation, resulting in quenching of $^1O_2$ and reduction in the UV absorbance of UA at its λmax 293 nm. The difference in UA absorbance (UA-A_{293}) of a photosensitizer solution in the dark and post irradiation can be used as photodynamic activity-indicating parameter [202, 203, 371]. It is worth noting that UA does not react detectably with hydrogen peroxide or superoxide anion which may be present in small amounts in an irradiated aqueous solution of UA and PS [363, 372].

3.2.1. Optimization of uric acid assay conditions

As MB has an absorption maximum in the UV range at 292 nm, overlapping the UA absorbance maximum at 293 nm (Figure 47), the working MB concentration range where MB absorbance does not override the difference in UA absorbance nm was determined before using the test. Figure 48 shows the effect light fluence (50 – 400 J/cm^2) on the reduction in UA absorbance (AU-A_{293}) at increasing MB concentration (2 - 12 µg/ml) upon irradiation of MB/UA solutions with a LED at 650 nm. Results showed that at all light fluences, values for (AU-A_{293}) increased up to a MB concentration of 4 µg/ml and then decreased, indicating that 4 µg/ml is the limiting value for MB concentration in the UA-based singlet oxygen assay. Moreover, it could be observed that the magnitude of the UA absorbance difference (AU-A_{293}) expressing $^1O_2$ generation at different MB concentrations generally increased by increasing the light intensity. A sample profile illustrating the change in AU-A_{293} for a MB solution 4 µg/ml is shown in Figure

49. Results indicated that singlet oxygen generation increased proportionally to the light intensity and leveled off at fluence exceeding 200 J/cm^2.

3.2.2. Photodynamic activity (PDA) of MB released from NFs

To assess the photodynamic activity of the MB-eluting NFs under study, a release experiment was conducted and samples of the release medium were subjected to the uric acid test for singlet oxygen assay after irradiation with a LED at 650 nm at two light fluences, 100 and 200 J/cm^2. In this range, $^1O_2$ was proportionate to light intensity. Release data obtained in PBS pH 7.4 at 37^{o}C for 6 h are shown in Figure 50. An initial increase in MB release for up to 2 h was followed by a plateau. Irradiation of samples of the release medium at different time intervals after 1:1 dilution with uric acid reagent (which reduced MB concentrations to less than 4 µg/ml) resulted in reduction in UA absorbance at 293 nm (UA-A_{293}). Similar UA-A_{293} values for solutions of released MB and MB drug substance (Table 12) indicated that the conditions of the emulsion electrospinning process did not affect the chemical integrity and photoactivation ability of MB.

Profiles for singlet oxygen generation in the release medium (expressed as UA-A_{293}) upon irradiation with LED at 50, 100 and 200 J/cm^2 over the 6 h-release duration are shown in Figure 51. Similarity of singlet oxygen generation and MB release profiles and the greater singlet oxygen generation at higher light dose indicated proportionality of MB photoactivity with the concentration of released MB and light fluence over this fluence range at constant light intensity (150 mW). Figure 52 shows sample UV/Vis spectra of UA and MB released at 2 h after irradiation with LED at 50, 100 and 200 J/cm^2. Photoactivation data coupled with photochemical integrity of MB released from NFs provide the basis for a new type of photoactive NFs with a photoactivation mechanism based on photosensitizer release. This implies that the photoactivity of these NFs depends on the release characteristics of the photosensitizer and the light fluence at a certain light intensity. MB-eluting NFs developed in the present study are different from polymer NFs doped with non-leachable water-insoluble photosensitizers with reported surface-restricted photoactivity upon irradiation [48, 373]. Photosensitization of these NFs is based on the generation and transport of $^1O_2$ within the fiber polymer matrix to the NFs surface. Accordingly, photoactivity of such NFs depends on the type of polymeric material and the transport of oxygen molecules to the excited photosensitizer [48, 373].

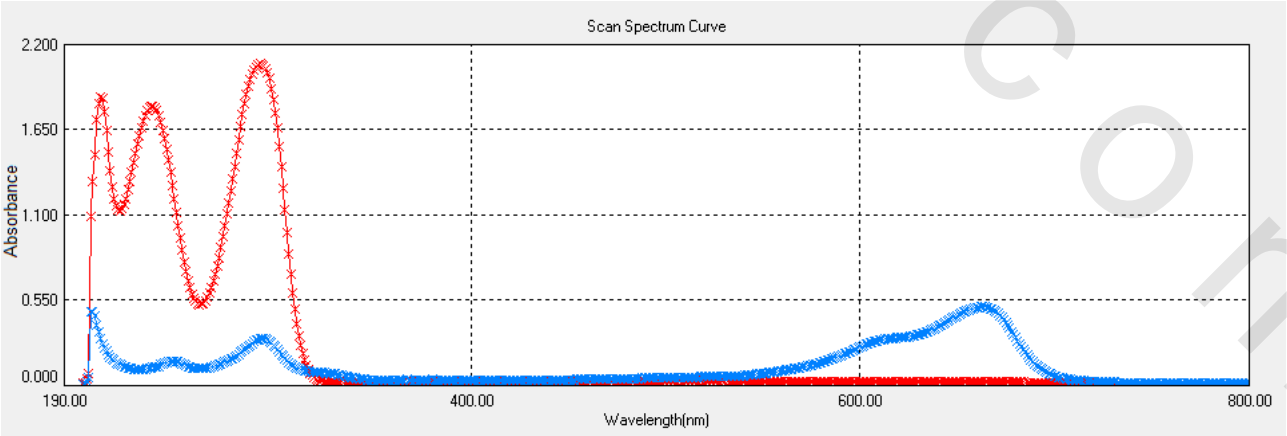

Figure 47: UV/Vis Spectra of uric acid (red) and MB (blue) aqueous solutions

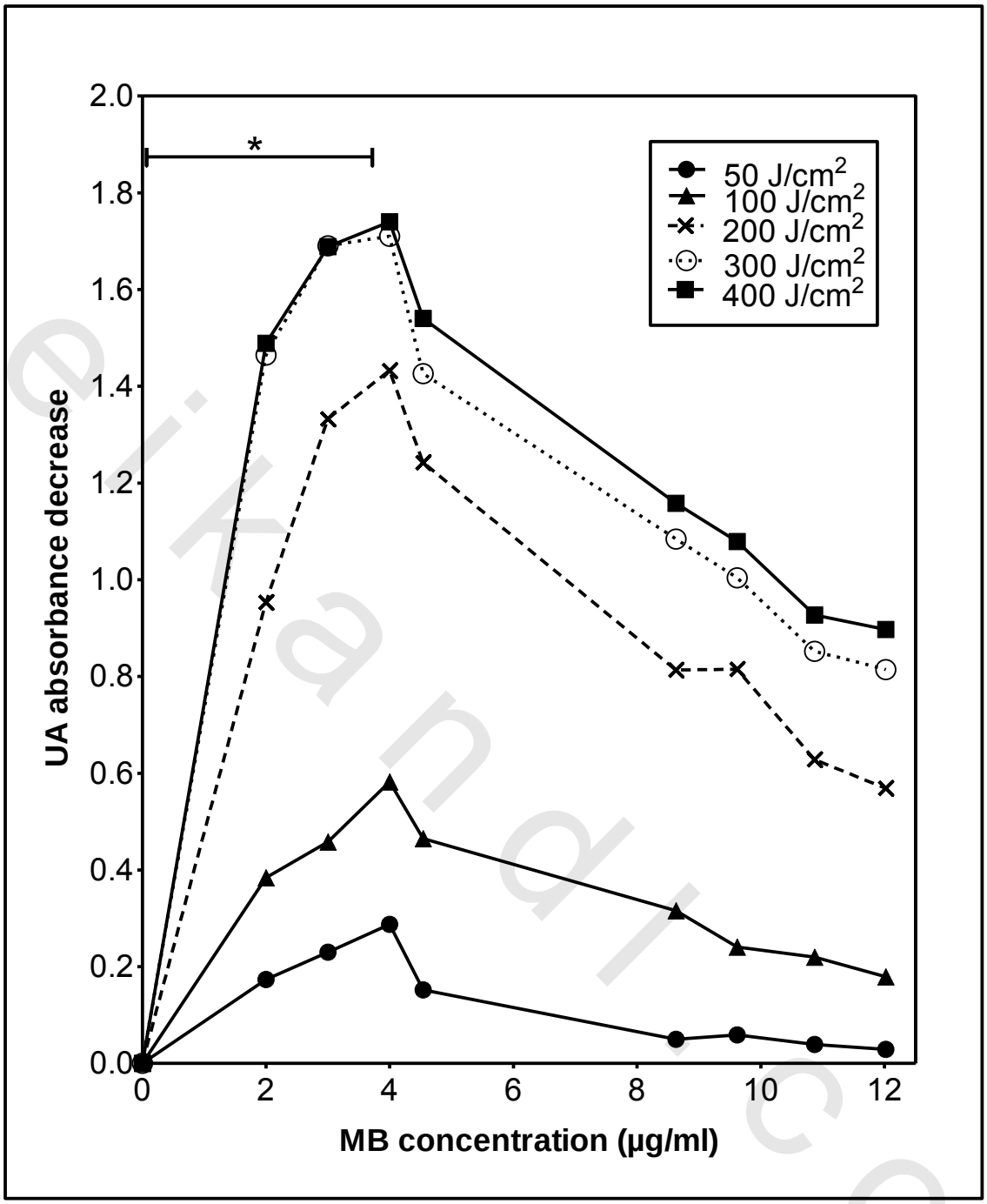

Figure 48: Effect of MB concentration and light fluence on uric acid absorbance decrease at 293 nm. LED at 650 nm was used for irradiation.

* The working MB concentration range for the test

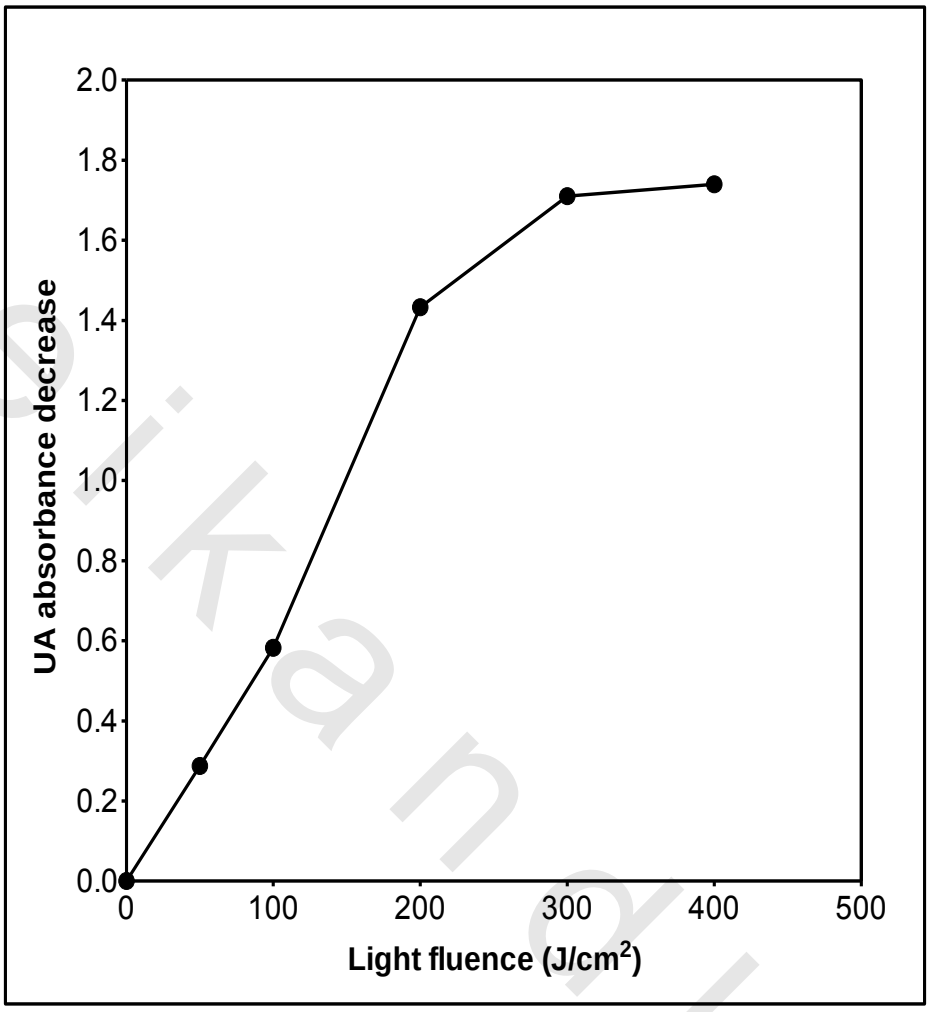

Figure 49: Change in decrease in uric acid (UA) absorbance at 293 nm in a MB solution (4 µg/ml) as a function of light fluence emitted by a LED at 650 nm

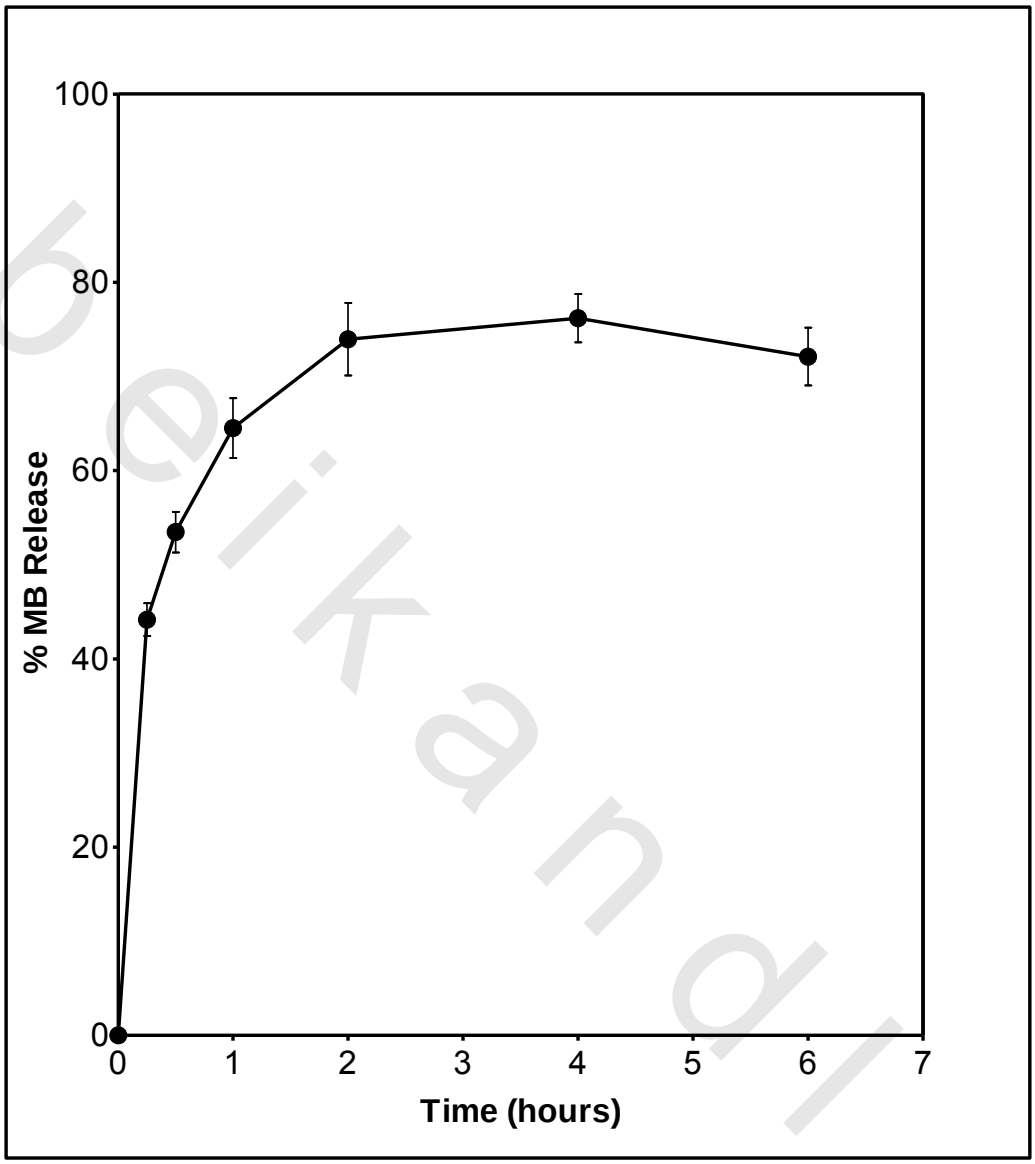

Figure 50: MB release over 6 h from PHB/PEG nanofibers in PBS at 37°C

.

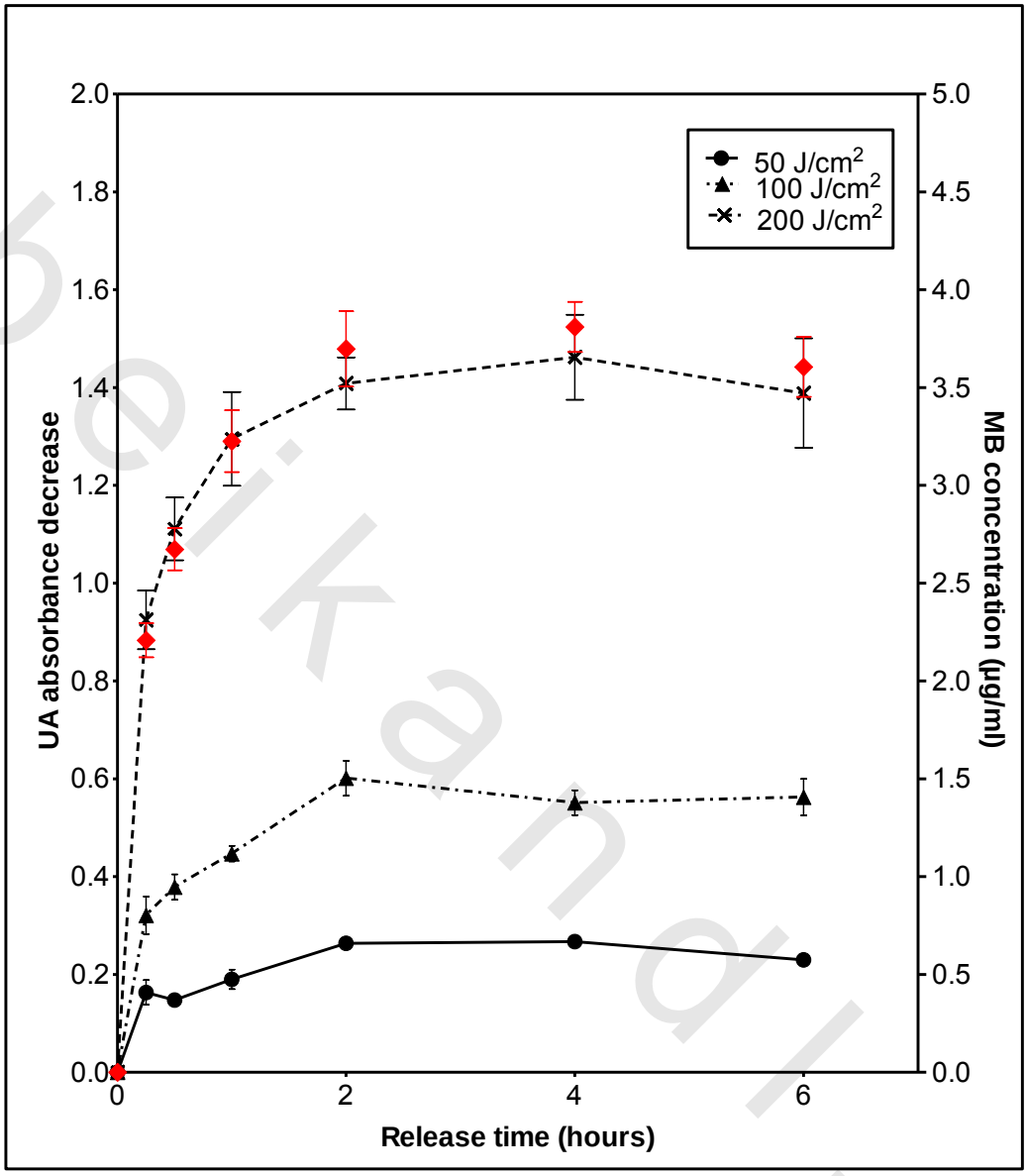

Figure 51: Uric acid absorbance decrease at 293 nm in response to singlet oxygen production upon irradiation of MB released at different time intervals from MB-PHB/PEG nanofibers. Received light doses: 50, 100 and 200 J/cm^2 using LED at 650 nm as light source.

*The red symbols are plotted on the right Y-axis to represent the concentration of MB (µg/ml) in the MB/uric acid solution mixture.

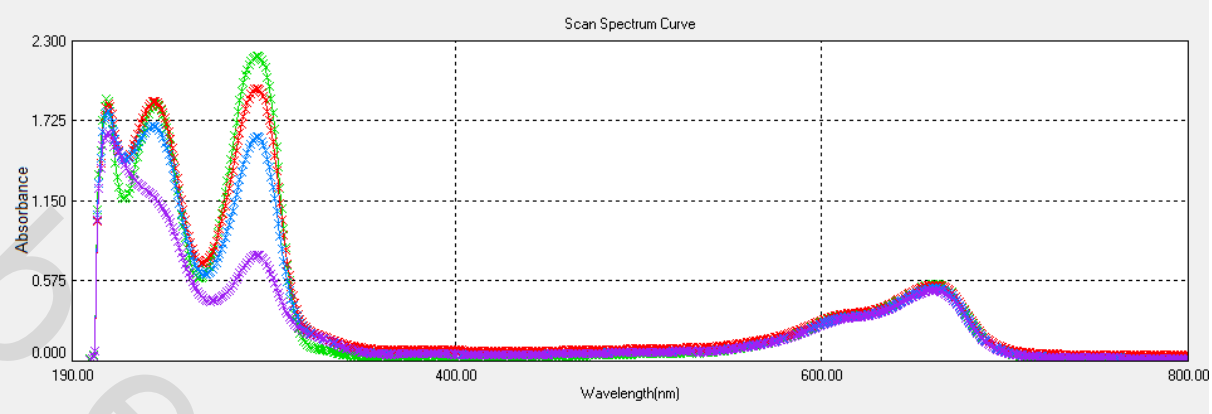

Figure 52: UV/Vis Spectra of uric acid and MB released (after 2 h) following irradiation with LED at 650 nm. Received light doses: 50 (red), 100 (blue) and 200 J/cm^2 (violet). The green spectrum is for uric acid and MB solution mixture in the dark.

3.3. Antimicrobial photodynamic activity (APDA) of MB-eluting PHB-PEG nanofibers

3.3.1. Antimicrobial Photodynamic activity (APDA) of MB solution

Based on data obtained so far, it could be hypothesized that the mechanism of antimicrobial activity of the MB-eluting NFs under study depends on the MB release and uptake by bacterial cells prior to irradiation. Accordingly, variables such as MB concentration, light fluence and pre-illumination incubation time with bacteria are primary determinants of the NFs APDA. The effect of modulating these variables on the photodynamic activity of MB solution was investigated to enable determination of optimal conditions for effective photodynamic activation of the NFs. Two staphylococcal bacterial strains were used, *staphylococcus aureus* standard strain (Sa_{st}) and MRSA, both commonly found in infected wounds [21].

Figure 53 and 54 show the surviving count of MRSA and Sa_{st} respectively exposed to different combinations of MB concentration in solution and light fluence compared to the surviving count of control bacteria not exposed to light. Light was applied following 30 min-incubation of MRSA with MB solution in all cases. Results indicated weak MB toxicity in the dark. As demonstrated in Chapter one of the thesis and reported in the literature [296], dark toxicity of antimicrobial photosensitizers requires prolonged incubation with bacteria. Exposure of bacterial suspensions to red light emitted by LED at 650 nm in the absence of MB had no killing effect on either strain. However, subjecting bacteria to combined treatment with MB and red light expectedly enhanced the antibacterial effect of MB in terms of speed and magnitude of killing. This can be attributed to the generation of a larger amount of $^1O_2$, causing greater damage that bacterial cells could not repair. The enhanced light activated antibacterial effect was generally dependent on MB concentration and the light fluence. For instance, a MB concentration of 25 µg/ml resulted in 2.5 and 3 $\log_{10}$ CFU reductions in the MRSA viable counts equivalent to 99.67 and > 99.99 % mean percentage killing at light fluences of 100 and 200 J/cm^2 respectively. A further increase in MB concentration to 50 µg/ml resulted in complete eradication of MRSA at both light fluences reaching a plateau which was maintained at 100 µg/ml. A similar pattern was generally observed for Sa_{st}. Increasing MB concentration at light fluences of 100 and 200 J/cm^2 resulted in enhanced bactericidal effect. A plateau was reached at 50 µg/ml MB, which was associated with > 99.99 % mean percentage kill at 100 J/cm^2 and complete eradication of bacteria at 200 J/cm^2.

As the photosensitizer concentration corresponding to the onset of plateau may be considered indicative of relative photobactericidal efficacy of the photosensitizer against the microorganisms destroyed [296], MB in the present study may be assumed to show a similar photobactericidal efficacy against the MRSA and Sa_{st} strains under study. However, a reduction in APDA of MB against Sa_{st} was observed upon increasing MB concentration to 100 µg/ml at 200 J/cm^2 (Figure 54). This can be explained by a self-shielding effect which occurs at relatively high PS concentrations [374]. This effect involves absorption of a significant proportion of the incident light applied to the bacterial suspension by the PS in solution, thus preventing sufficient light reaching the PS-loaded cells.

Apart from MB concentration and light fluence, pre-illumination incubation of the bacteria with the PS is a main parameter of APDA. Incubation with the microorganism for sufficient time

before illumination allows for more cellular uptake of the PS [375, 376]. As ROS have a short half-life and act close to their site of generation, only molecules and structures that are proximal to the area of ROS production (areas of PS localization) are directly affected by photodynamic activity [154]. Accordingly, the pre-illumination incubation time may contribute to differences in the cellular localization of the PS [296, 376]. This is particularly relevant to MB which is known to exert its antimicrobial effect by primarily damaging bacterial cell DNA and to a lesser extent the outer membrane [295].

In the present study, the effect of pre-illumination incubation time on the APDA of MB was assessed using two MB concentrations (25 and 50 µg/ml) and 100 J/cm^2 light fluence. Results are shown in Figure 55. Increasing the pre-illumination incubation time enhanced bacterial killing at both MB concentrations, a plateau being reached at 15 min. A longer pre-illumination incubation time did not affect photoactivity. It should be noted that the killing effect observed at zero pre-illumination incubation time is attributed to MB released during light irradiation for 25 min to produce the 100 J/cm^2 light fluence required.

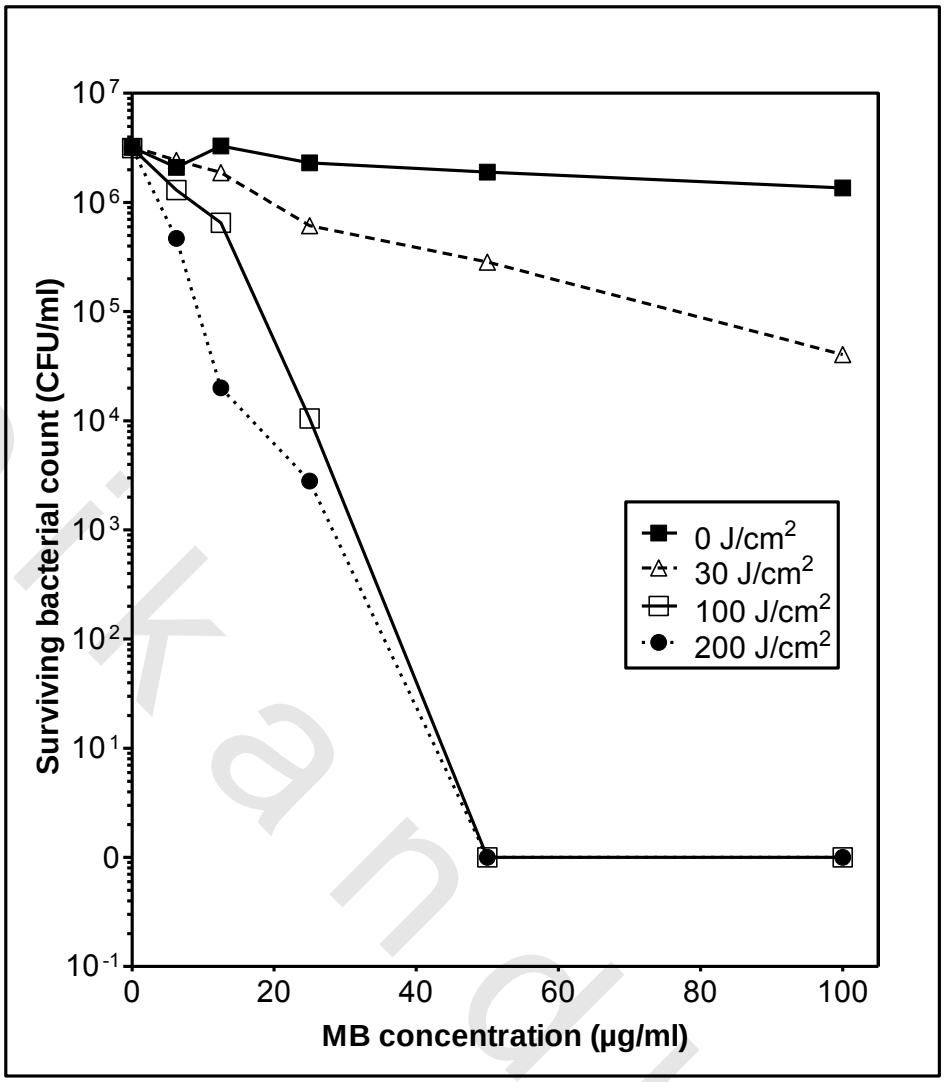

Figure 53: Effect of light fluence at 650 nm and MB solution concentration incubated with ~ 10^6 CFU/ml MRSA on mean surviving bacterial count using the viable count technique.

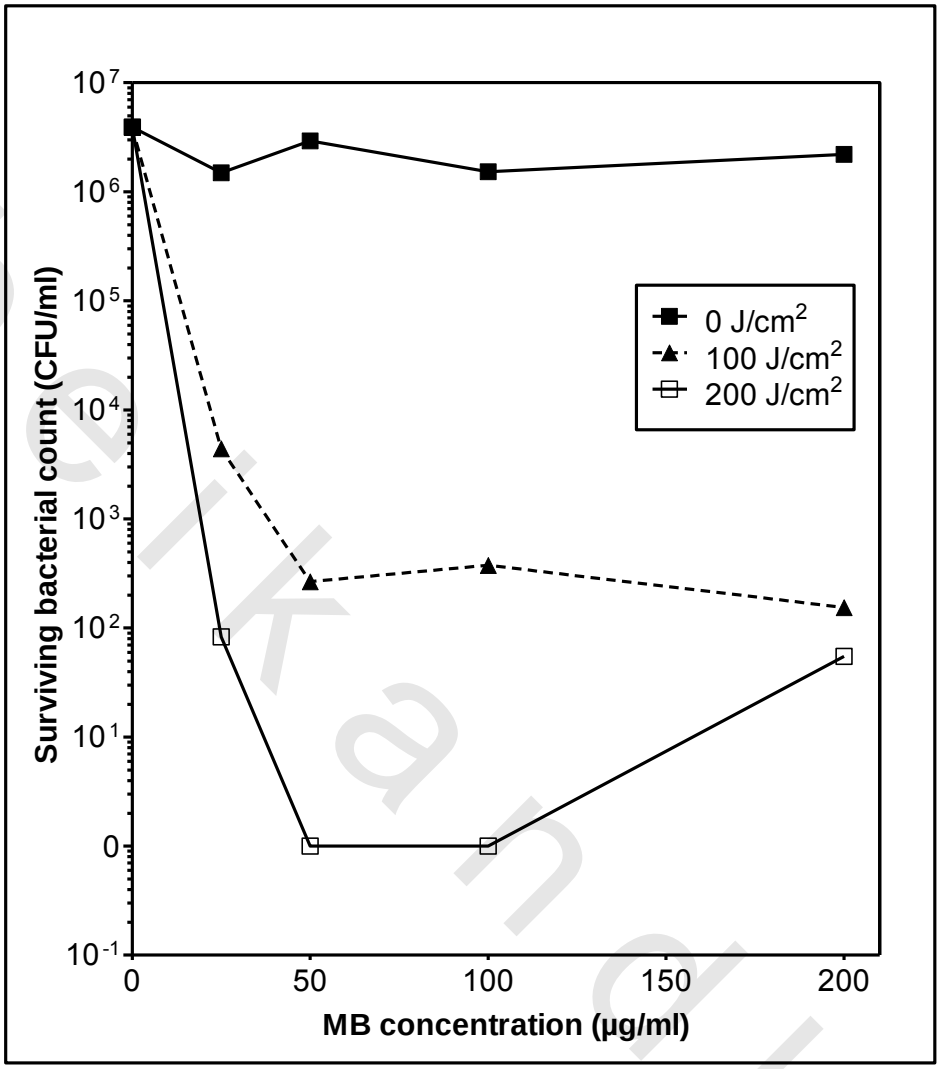

Figure 54: Effect of LED light fluence at 650 nm and MB solution concentration on the mean surviving bacterial count using the viable count technique (Initial Sa_{st} inoculum size ~ 10^6 CFU/ml)

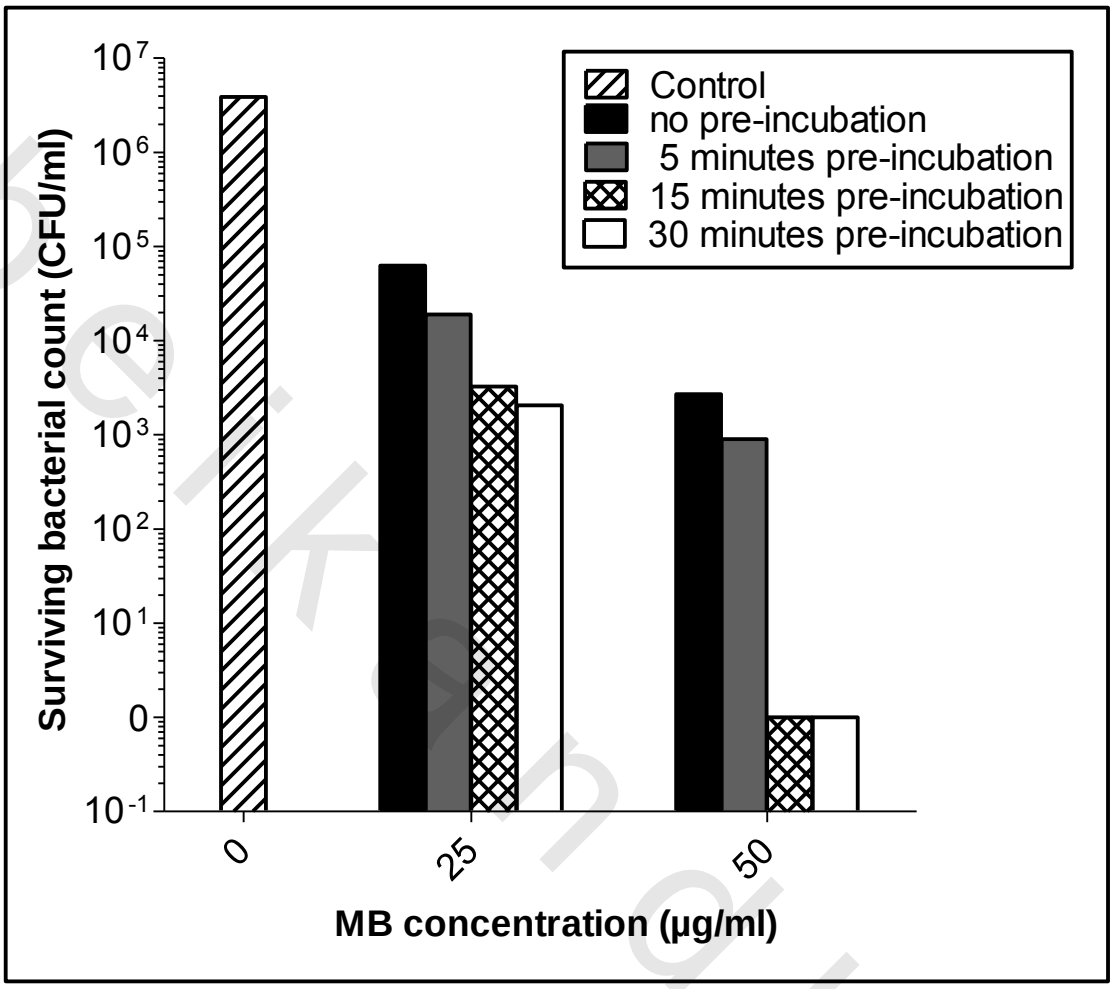

Figure 55: Effect of incubation time of MRSA (~ 10^6 CFU/ml) in MB solution (25 and 50 µg/ml) on surviving bacterial count upon illumination with LED at 100 J/cm^2 using the viable count technique.

3.3.2. Antimicrobial Photodynamic activity (APDA) of MB-eluting NFs

The antibacterial activity of MB-eluting NFs under study was assessed against MRSA and Sa_{st} using the viable count technique and compared to MB solution equivalent to that released from the NFs according to a previous release study in the presence of bacteria (Figure 30, chapter 1). Samples were irradiated with red light at 100 J/cm^2 after an incubation period of 15 min. Bacterial counts were performed after illumination and compared to controls kept in the dark. Instantaneous killing for both organisms was observed after illumination as shown in Figure 56. The NFs systems exerted a greater killing effect compared to MB solution which was more pronounced against MRSA relative to Sa_{st}. The greater APDA of NFs can be attributed to the large surface area of MB-eluting NFs which may enhance interaction with MB and uptake by bacterial cells.

An interesting characteristic of the MB-eluting NFs under study is the dual antimicrobial / photosensitizing action exerted by MB. This may offer great promise in antimicrobial applications as the instant bactericidal effect produced by light-activation of the early released MB can be sustained by the dark toxicity of MB released progressively under the temporal control of NFs. This assumption was verified by testing the APDA of MB-NFs against MRSA and Sa_{st} in nutrient broth rather than saline. After illumination at 100 J/cm^2, test bacterial suspensions were subjected to counting for instant killing effect while control suspensions were maintained in nutrient broth in the dark for 24 h post illumination to test for bacterial growth. Results are shown in Figure 57. Illumination of MB-loaded NFs incubated with both organisms resulted in instantaneous killing effect that exceeded 99.99 and 99.95 % mean killing for MRSA and Sa_{st} respectively. Furthermore, complete clearance of both organisms was observed after 24 h, indicating effective bactericidal activity of MB with no chance for bacterial recovery most probably due to progressive MB release.

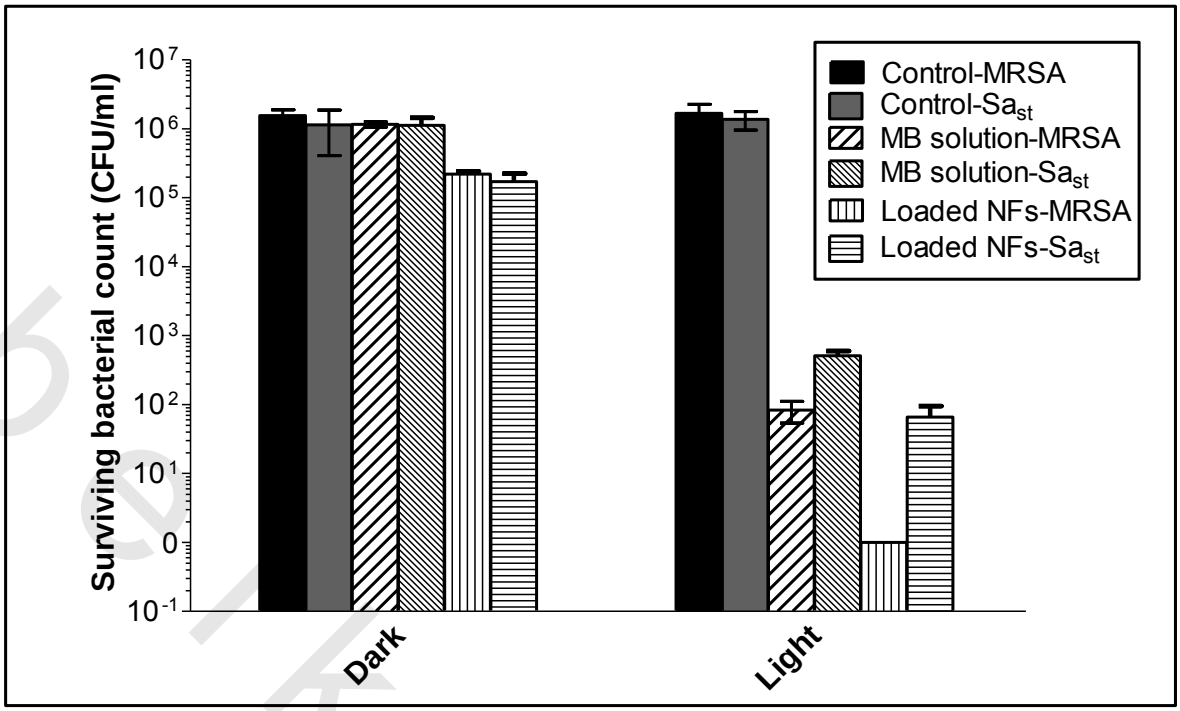

Figure 56: Antibacterial photodynamic activity of MB-eluting PHB/PEG nanofibers against MRSA and Sa_{st} (~ 10^6 CFU/ml) in comparison with MB solution, using the viable count technique.

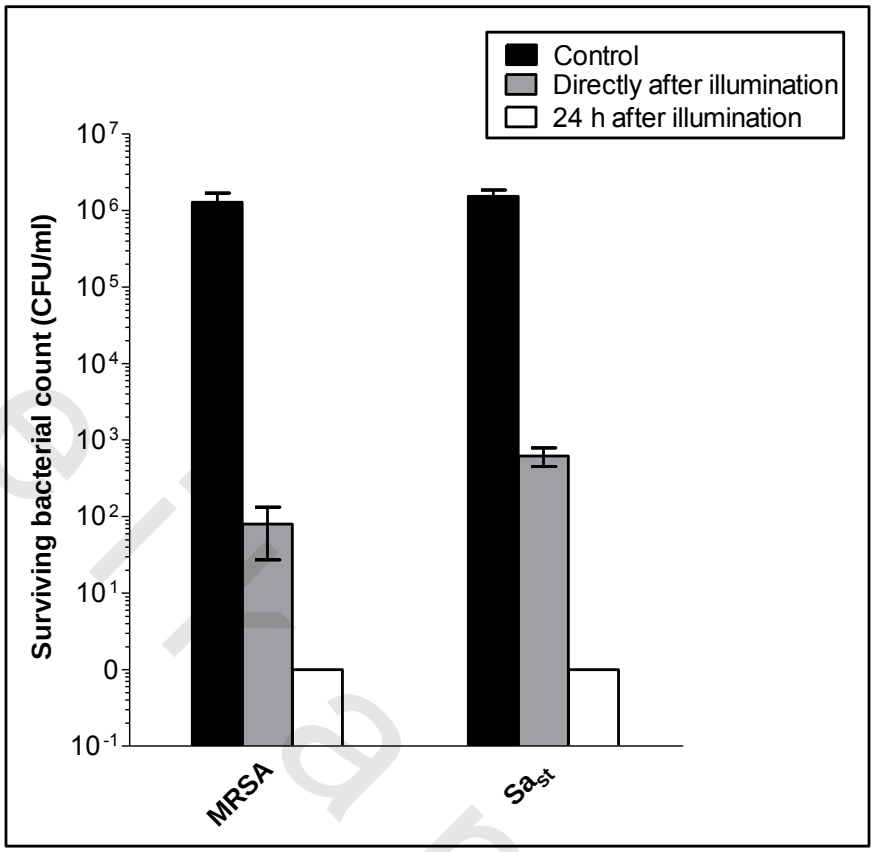

Figure 57: Bactericidal activity of MB-eluting PHB/PEG nanofibers against MRSA and Sa_{st} (~ 10^6 CFU/ml) using the viable count technique.

4. Conclusion

MB-eluting PHB/PEG nanofibers are presented as a biomaterial for photodynamic antimicrobial applications combining the multiple functional and structural features of NFs and antimicrobial activity of MB as both antimicrobial agent and photosensitizer. The mechanism of photodynamic activation depends on photosensitizer release rather than transport of ROS which is in harmony with the mechanism of bacterial destruction by MB, based primarily on cellular uptake and DNA damaging. Both the polymer matrix and MB contribute to the enhancement of the antimicrobial profile of photoactivated MB-PHB/PEG NFs. Apart from the well-established role of nanofibers as scaffold for cell regeneration and accelerated wound healing, the opaque PHB/PEG blend NFs probably protect the entrapped MB from unintended photosensitization and provide temporal control over its localized delivery at the infection site. This allows for single or multiple light irradiation for instant bacterial killing and prolonged duration of the sustained dark antimicrobial effect of MB. Data obtained provide evidence for the potential of the MB-eluting PHB/PEG nanofibers in short term antimicrobial applications. These *in vitro* data should be substantiated with *in vivo* assessment of MB-eluting nanofibers as wound healing matrices with potential clinical applicability. This is the subject of the Chapter 4.